Femtosecond Laser-Induced Damage and Filamentary Propagation in Fused Silica

L. Sudrie,[1] A. Couairon,[2] M. Franco,[1] B. Lamouroux,[1] B. Prade,[1] S. Tzortzakis,[1] and A. Mysyrowicz[1]

[1]*Laboratoire d'Optique Appliquée, École Nationale Supérieure des Techniques Avancées–École Polytechnique, F-91761 Palaiseau Cedex, France*

[2]*Centre de Physique Théorique, CNRS UMR 7644, École Polytechnique, F-91128 Palaiseau Cedex, France*

(Received 3 May 2002; published 15 October 2002)

Bulk damage induced by fs IR laser pulses in silica is investigated both experimentally and numerically. In a strong focusing geometry, a first damage zone is followed by a narrow track with submicron width, indicating a filamentary propagation. The shape and size of the damage tracks are shown to correspond to the zone where the electron density created by optical field ionization and avalanche is close to 10^{20} cm^{-3}. The relative role of avalanche and photoionization is studied. The plasma density produced in the wake of the pulse is shown to saturate around 2–4 $\times$ 10^{20} cm^{-3}.

DOI: 10.1103/PhysRevLett.89.186601 PACS numbers: 72.20.Jv, 42.65.Sf, 61.80.Ba, 79.20.Ds

From micromachining of optical materials [1–4] to biomedical technologies [5], from femtochemistry to data storage [6,7], lasers delivering ultrashort pulses will find a large number of potential applications, for which the controlled deposition of laser energy in solids is crucial.

A large number of experimental and theoretical studies have been conducted to understand the mechanisms of laser damage (see [8,9] and references therein). For picosecond or longer pulses, bulk damage inside defect-free dielectrics involves the heating and multiplication of spurious electrons by the incident laser beam and transfer of this energy to the lattice. Damage occurring via this conventional heat deposition results in the melting and boiling of an extensive volume of the dielectric material. The situation is quite different for femtosecond pulses which are shorter than the time scale for electron energy transfer to the lattice [8,10]. Damage caused by these pulses is produced with smaller statistical uncertainty and is controllable on a microscopic scale. It is characterized by a minimum of collateral damage. These properties can be exploited to produce laser devices such as arrays of damage dots for all optical memories with high data storage density [6], longitudinal grooves forming waveguides [2,3], or arrays of parallel grooves to form transmission gratings [11,12]. Understanding in detail the mechanisms of laser-solid interaction leading to damage in the bulk of dielectrics becomes, therefore, an essential issue. In the literature, however, most of the experiments on damage to dielectrics were done on surfaces. In this way, the difficulty of interpretation associated with nonlinear propagation of the pulse in the material was avoided.

The goal of this Letter is to present the first theoretical understanding of damage induced in the *bulk* of fused silica by interaction with *femtosecond* infrared laser pulses. By means of a numerical code that describes not only the propagation of laser pulses in fused silica, but also the generation of an electron plasma by photoionization (PI) and avalanche and the subsequent defocusing of the pulse, we investigate the link between the damage tracks and femtosecond filamentation. We accurately relate the electron density reached near the nonlinear focus of the beam to the shape and size of the damage tracks examined by scanning electron microscopy. We show that fs laser pulses propagating in silica generate an electron plasma with a saturated density in the range 1–3 $\times$ 10^{20} cm^{-3}, well below the critical plasma density 2 $\times$ 10^{21} cm^{-3}, and induce bulk damage of controllable shape and size.

When a laser pulse with input power larger than the critical power for self-focusing $P_{\mathrm{cr}} = \lambda_0^2/2\pi n_0 n_2$ propagates in a Kerr medium such as fused silica, a catastrophic collapse is predicted to occur at a finite distance z_c [13]. Here λ_0, n_0, and n_2 denote the laser wavelength in vacuum, the linear and the nonlinear refraction index of fused silica, respectively. Actually, the collapse is prevented by free carrier generation which decreases the refractive index. Instead, a dynamic balance between self-focusing and PI leads to a filamentary propagation characterized by a near constant beam waist over many Rayleigh lengths [14], similar to the fs light filaments produced in air with powerful laser beams [15–21]. Very high local intensities prevail in the filament, in excess of 10^{13} W/cm^2, but the pulse duration is too short to initiate avalanche so that no permanent damage is observed in the bulk. This situation where the material seems to withstand the generation of damage will be referred to as the case of weak focusing, for which the focus length is larger than the self-focusing distance z_c [22].

Despite this remarkable resistance to optical breakdown and material damage in the interaction of fs pulses with bulk optical materials, extensive damage is produced in the bulk in a strong focusing geometry. Figure 1(a) shows a magnified photograph of bulk damage induced by exposing fixed points of a silica plate during 2 s to the focused laser beam with a peak power of 7.8 MW and a pulse duration of 160 fs, measured from an autocorrelation trace. Damage tracks obtained under the above

 © 2002 The American Physical Society

conditions have been observed under an optical microscope along the propagation axis. A first damage zone of a few tens of microns is shown in Fig. 1(a). A second long filamentary track with a diffraction limited width extending up to 80 μm appears beyond the first damage zone.

To produce these tracks, we used a regenerative amplified Ti:Sapphire fs laser operating at $\lambda_0 = 800$ nm, at a repetition rate of 200 kHz, with a maximum energy per pulse of $E_{\text{in}} = 2$ μJ. The beam was focused 450 μm inside a fused silica sample with a microscope objective of numerical aperture NA = 0.5. The waist of the focal spot $w_f = 1$ μm was measured from a low intensity shot. The sample could be translated along three orthogonal axes by computer controlled stepping motors.

In order to have a better spatial resolution, we have also examined the damaged zone under a scanning electron microscope (SEM). Although a SEM cannot reveal permanent index changes of the material, it can, however, reveal fractures with a resolution down to 10 nm, whereas the resolution of the optical microscope is diffraction limited. Adjacent damage tracks were induced along the propagation z axis by exposing a sample moving at constant speed 100 μm/s along y. We have examined the extent of these tracks by cleaving the fused silica plate along an x-z plane. The plate was then recovered by a thin gold layer in thermal expansion so as to obtain a conductive surface ready to view the tracks under a SEM. As shown in Fig. 2(a), a damage track consists of a diffusing zone of length 25 ± 4 μm and width 3.7 ± 0.5 μm, followed by a second narrower track.

For the numerical simulations, we model the linearly polarized beam with cylindrical symmetry around the propagation axis z by the envelope $\mathcal{E}$ of the electric field $\mathbf{E}$, written as $\mathbf{E} = \text{Re}[\boldsymbol{\mathcal{E}} \exp(ikz - i\omega_0 t)]$, where $k = n_0\omega_0/c$ and ω_0 are the wave number and frequency of the carrier wave and $n_0 = 1.45$ for fused silica. The input beams were modeled by Gaussians with input power $P_{\text{in}} = E_{\text{in}}/t_p\sqrt{\pi/2}$ and intensity $\mathcal{E}_0^2 = 2P_{\text{in}}/\pi w_0^2$, where E_{in} denotes the input energy and the temporal FWHM diameter was 160 fs (temporal half width $t_p = 136$ fs):

$$\mathcal{E}(r, t, 0) = \mathcal{E}_0 \exp(-r^2/w_0^2 - t^2/t_p^2 - ikr^2/2f). \quad (1)$$

They exhibit a transverse waist $w_0 = w_f(1 + d^2/z_f^2)^{1/2}$ where $w_f = 1$ μm is the beam waist, $z_f = \pi w_f^2 n_0/\lambda_0 = 5.7$ μm the Rayleigh length, and $f = d + z_f^2/d$ the curvature of the wave at the distance d from the linear focus (we start our simulations $d = 75$ μm from the focus). The scalar envelope $\mathcal{E}(r, t, z)$ is assumed to be slowly varying in time and along z. It evolves according to the propagation equation expressed in the reference frame moving at the group velocity $v_g \equiv \partial\omega/\partial k|_{\omega_0}$:

$$\frac{\partial \mathcal{E}}{\partial z} = \frac{i}{2k}\left(\frac{\partial^2}{\partial r^2} + \frac{1}{r}\frac{\partial}{\partial r}\right)\mathcal{E} - i\frac{k''}{2}\frac{\partial^2 \mathcal{E}}{\partial \tau^2} + ik_0 n_2 |\mathcal{E}|^2 \mathcal{E} - \frac{\sigma}{2}(1 + i\omega_0\tau_c)\rho\mathcal{E} - \frac{1}{2}\frac{W_{\text{PI}}(|\mathcal{E}|)U_i}{|\mathcal{E}|^2}\mathcal{E}, \quad (2)$$

where τ refers to the retarded time variable $t - z/v_g$. The terms on the right-hand side of Eq. (2) account for diffraction in the transverse plane, group velocity dispersion with coefficient $k'' \equiv \partial^2 k/\partial\omega^2|_{\omega_0} = 361$ fs^2/cm, self-focusing related to the Kerr effect occurring for pulses with P_{in} above $P_{\text{cr}} = 1.82$ MW ($n_2 = 3.54 \times 10^{-16}$ cm^2/W for fused silica), plasma absorption (PLA), defocusing with electron density ρ, and photoabsorption (PA) of energy necessary for the PI of the medium. For PLA, the cross section for inverse bremsstrahlung follows the Drude model [9] and reads $\sigma = k\omega_0\tau_c/n_0^2\rho_c(1 + \omega_0^2\tau_c^2) = 1.55 \times 10^{-18}$ cm^2, where $\tau_c = 2.33 \times 10^{-14}$ s. The quantity $n_0^2\rho_c = 2.3 \times 10^{21}$ cm^{-3} denotes the critical plasma density above which the plasma is opaque.

An evolution equation for the electron density ρ describe the PI processes involving transition from the valence band to the conduction band [8,10], through the gap potential $U_i = 9$ eV in silica.

$$\partial\rho/\partial t = W_{\text{PI}}(|\mathcal{E}|) + \eta\rho|\mathcal{E}|^2 - \rho/\tau_{\text{r}}. \quad (3)$$

The first term on the right-hand side of Eq. (3) describes the PI contribution to free electron generation, while the second term accounts for avalanche ionization with $\eta = \sigma/U_i$. The third term represents electron recombination with a characteristic time $\tau_{\text{r}} = 150$ fs in fused silica [23].

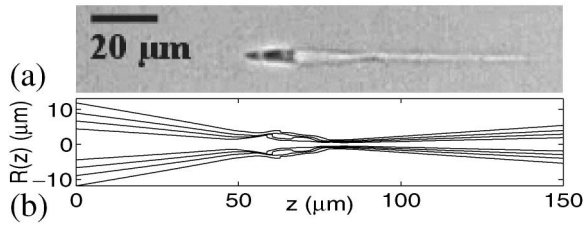

FIG. 1. (a) Magnified photograph of damage tracks viewed along the propagation axis of the pulse. (b) Beam radius vs z, for the fractions 55%, 65%, 75%, and 85% of $F[R(z), z]/\max[F(r, z)]$, where F denotes the fluence.

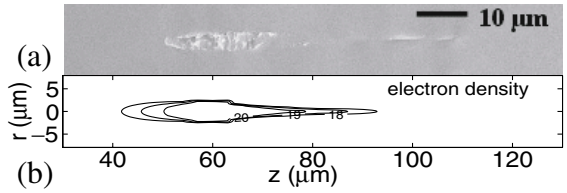

FIG. 2. (a) Damage tracks in fused silica viewed under a scanning electron microscope. (b) Contour plot of the computed electron density at levels 10^{18}, 10^{19}, and 10^{20} cm^{-3}.

Following Keldysh's [24] formulation for the PI rate W_{PI}, we define the adiabaticity parameter for solids $\gamma = \omega_0\sqrt{mU_i}/e\mathcal{E}$, where $m = 0.635m_e$ denotes the reduced mass of the electron and the hole; γ is equal to unity for an intensity $I = 3.5 \times 10^{13}$ W/cm^2. In our simulations, I reaches 5×10^{13} W/cm^2 near the focus for $E_{\mathrm{in}} = 1$ μJ. Therefore, the PI rate that can neither be reduced to the tunnel formula valid for $\gamma \ll 1$ nor to the multiphoton rate prevailing for weak fields $\gamma \gg 1$ reads:

$$W_{\mathrm{PI}}(|\mathcal{E}|) = \frac{2\omega_0}{9\pi}\left(\frac{\omega_0 m}{\hbar\sqrt{\Gamma}}\right)^{3/2} Q(\gamma, x)\exp(-\alpha\langle x+1\rangle), \quad (4)$$

where $\Gamma = \gamma^2/(1+\gamma^2)$, $\Xi = 1-\Gamma$, $Q(\gamma, x) = \sqrt{\pi/2K(\Xi)} \times \sum_{n=0}^{\infty}\exp(-n\alpha)\Phi[\sqrt{\beta(n+2\nu)}]$, $\alpha = \pi\frac{K(\Gamma)-E(\Gamma)}{E(\Xi)}$, $\beta = \frac{\pi^2}{4K(\Xi)E(\Xi)}$, $x = \frac{2}{\pi}\frac{U_i}{\hbar\omega_0}\frac{1}{\sqrt{\Gamma}}E(\Xi)$, $\nu = \langle x+1\rangle - x$, $\langle\cdots\rangle$ denotes the integer part, K and E denote the complete elliptic integral of the first and second kind, and Φ the Dawson function $\Phi(z) = \int_0^z \exp(y^2 - z^2)dy$.

Figure 3 shows the ionization rate W_{PI} for silica as a function of the laser intensity. It approaches asymptotically Keldysh's multiphoton rate (dotted curve) and tunnel ionization rate (dash-dotted curve) at the extreme limits of weak and strong fields. For weak fields, Keldysh's theory coincides with the multiphoton ionization rate $W_{\mathrm{MPI}} = \sigma_6 I^6 \rho_{\mathrm{at}}$ (dashed line), where $\sigma_6 = 9.8 \times 10^{-70}$ cm^{12}/W^6 denotes the coefficient for silica and $\rho_{\mathrm{at}} = 2.1 \times 10^{22}$ cm^{-3}, the background atom density. At $I = 3.5 \times 10^{13}$ W/cm^2 ($\gamma = 1$), $W_{\mathrm{MPI}} = 4.1 \times 10^{34}$ cm^{-3} s^{-1} clearly overestimates the PI rate $W_{\mathrm{PI}} = 1.6 \times 10^{32}$ cm^{-3} s^{-1} by 2 orders of magnitude. This is the reason why σ_6 is taken to be smaller in [10] ($\sigma_6 = 1.5 \times 10^{-71}$ cm^{12}/W^6), but larger values are also used ($\sigma_6 = 3 \times 10^{-67\pm0.9}$ cm^{12}/W^6 [25]). Our simulations were realistic only with the PI rate (4).

Before showing the link between the damage tracks and the computed electron density, we comment Fig. 1(b). It shows various radius of the beam $R(z)$, measured numerically as the widths at different levels of the maximum of the fluence distribution, defined as $F(r, z) = \int_{-\infty}^{+\infty}|\mathcal{E}(r, z, t)|^2 dt$. The focusing stage is followed by a slightly defocusing stage induced by the excitation of an electron plasma near the focus. This zone coincides with the first damage track. A beam refocusing then clearly occurs and leads to a filamentary propagation that induces a local isotropic increase of the refraction index along the filamentary track over a lateral dimension of a few microns. As shown in [26], this type of damage can be cured by heating the sample to 900 °C, whereas this is not true for the first damage zone.

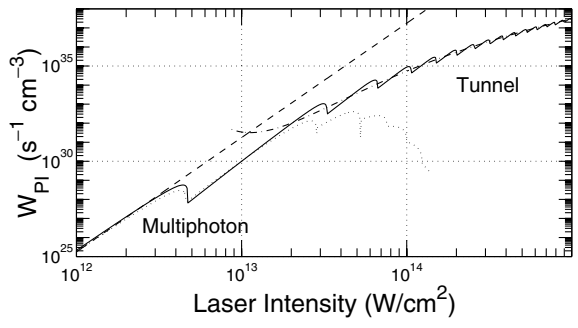

FIG. 3. Ionization rate for fused silica with gap $U_i = 9$ eV from Keldysh's theory (solid line), in the tunnel (dash-dotted line), and multiphoton (dotted line) limits. The multiphoton rate $W_{\mathrm{MPI}} = \sigma_6 I^6 \rho_{\mathrm{at}}$ is shown as a dashed line.

We then examine this filamentary structure under high SEM resolution. The filamentary track has nearly disappeared, except for thin fracture zones, 200–400 nm in diameter, extending up to 80 μm [see Fig. 2(a)]. They are attributed to beam refocusing during filamentary propagation. This corroborates the fact that a permanent index change was responsible for the appearance of the thin track shown in Fig. 1(b). The result is in agreement with Bloembergen's prediction that the damage track should be thinner than the size of the light filament [27]. Measurements of the absorption of energy in the silica plate have confirmed that the output power after propagation in the plate is still larger than P_{cr}.

Next we discuss the first damage zone. Its shape and length is closely related to the domain where the electron density computed from our code exceeds 3×10^{20} cm^{-3}, as shown in Fig. 2(b) where various density levels computed in the wake of the pulse are plotted as functions of r and z. The density level at 10^{20} cm^{-3} is indeed 28 ± 1 μm long and 4.3 ± 0.5 μm wide in good quantitative agreement with the extent of the damage track shown in Fig. 2(a).

Figure 4 details the relative role of PI and avalanche in the damage process. The maximum electron density reached in the damage zone saturates at a nearly constant value clamped to 2–4 $\times 10^{20}$ cm^{-3}, when the input energy of the pulse varies [solid curve in Fig. 4(a)]. This density is 1 order of magnitude below the critical density 2.3×10^{21} cm^{-3}. Even when the input energy increases, this is supported by the lack of a reflected signal that we have carefully looked for by means of pump probe experiments. The same saturation effect occurs in the case of a weak focusing in fused silica where long filaments are observed [14]. In this case, however, no associated damage was observed because the electron density was clamped to 10^{19} cm^{-3}. The dashed curve in Fig. 4(a) shows the same quantities when only PI is taken into account: the saturated density is then clamped to values between 2×10^{19} and 10^{20} cm^{-3}. The main part of the electron density in this strong focusing geometry is therefore obtained through the avalanche process. Avalanche, however, becomes significant only when the density of electrons created by PI exceeds 10^{19} cm^{-3}. Since PI determines the threshold which triggers avalanche, it was crucial to use the complete Keldysh's formulation for the PI rate in order to estimate quantitatively this avalanche threshold.

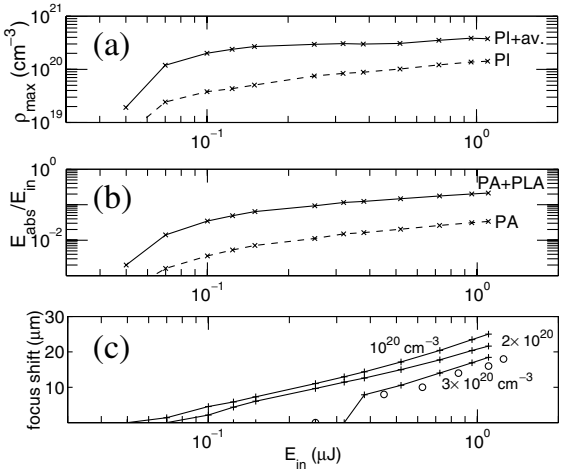

FIG. 4. (a) Electron density, (b) energy losses, (c) focus shift computed from our code (curves) and border of the damage tracks measured experimentally [open circles in (c)] as a function of the input energy. PI: photoionization. av: avalanche. PA : photoabsorption. PLA: plasma absorption.

Figure 4(b) shows the energy losses due to PA only (dashed curve) and to both PA and PLA (solid curve) as a function of the pulse energy. The main part of the absorption is due to PLA. It was therefore important to estimate this effect correctly. We have tried to use Thornber's model [28–30] instead of the Drude/Stuart's [9] model for avalanche and PLA rates. It takes into account the effects of ionization scattering, optical phonon scattering, and thermal scattering in one mean free path. For large intensities, the PLA coefficient $\eta(I) \times I$ becomes proportional to the electric field and not to the intensity as in Drude's model [for weak intensities $\eta(I) \times I$ is still proportional to $|\mathcal{E}|$ with a different slope]. For large input energies, the transmission computed with Thornber's model was found to be too large compared to the experimental measurements. In addition, for low input energies, absorption was too large leading to an unrealistic threshold in energy for triggering avalanche with Thornber's model. A much better quantitative agreement between numerics and experiments was obtained with the Drude's model. Figure 4(c) summarizes the results predicted by our numerical model for the focus shift, defined as the difference between the focal distance and that at which the density exceeds 1, 2, or 3 times 10^{20} cm^{-3}. The circles in Fig. 4(c) show the difference between the focal distance and the distance at which the damage is visible. These experimental data are nearly superposed to the focus shift evaluated numerically for an electron density of 3×10^{20} cm^{-3}, close to the value deduced from the analysis of the shape of the damage.

In conclusion, we have provided the first detailed understanding of the mechanisms responsible for bulk damage induced by the propagation of fs laser pulses in fused silica. By postmortem inspection of the material, we characterized the damage tracks and we found that the shape of the principle track is very well reproduced by the domain where the electron density computed by considering Keldysh's PI rate, avalanche, and recombination saturates around 3×10^{20} cm^{-3}. From our model, the control of the refraction index changes on a submicron scale in the damage zone can be achieved to produce damage-resistant laser devices. This model generally applies to fs filamentation in other media as, e.g., air, for which an absorption threshold plays the role of the damage threshold in silica. When the plasma in air becomes strongly absorbing, exciting prospects associated with long range filamentation such as remote sensing in the atmosphere [19] and lightning protection [20] become problematic.

We gratefully acknowledge the invaluable help of A. Alexandrou, B. Poumellec, P. Mora, and the expertise of P. Riberty in performing scanning electron micrographs.

[1] M. Lenzner, J. Krüger, W. Kautek, and F. Krausz, Appl. Phys. A **68**, 369 (1999).
[2] K. M. Davis, K. Miura, N. Sigumoto, and K. Hirao, Opt. Lett. **21**, 1729 (1996).
[3] D. Homoelle *et al.*, Opt. Lett. **24**, 1311 (1999).
[4] C. B. Schaffer, A. Brodeur, J. F. Garcia, and E. Mazur, Opt. Lett. **26**, 93 (2001).
[5] F. H. Loesel *et al.*, Appl. Phys. B **66**, 121 (1998).
[6] E. N. Glezer *et al.*, Opt. Lett. **21**, 2023 (1996).
[7] M. Watanabe *et al.*, Jpn. J. Appl. Phys. **37**, L1527 (1998).
[8] B. C. Stuart *et al.*, Phys. Rev. Lett. **74**, 2248 (1995).
[9] B. C. Stuart *et al.*, Phys. Rev. B **53**, 1749 (1996).
[10] M. Li, S. Menou, J. P. Nibayer, and G. N. Gibson, Phys. Rev. Lett. **82**, 2394 (1999).
[11] Y. Kondo *et al.*, Opt. Lett. **24**, 646 (1999).
[12] L. Sudrie, M. Franco, B. Prade, and A. Mysyrowicz, Opt. Commun. **171**, 279–284 (1999).
[13] Y. R. Shen, *The Principles of Nonlinear Optics* (Wiley, New York, 1984).
[14] S. Tzortzakis *et al.*, Phys. Rev. Lett. **87**, 213902 (2001).
[15] A. Braun *et al.*, Opt. Lett. **20**, 73 (1995).
[16] E. T. J. Nibbering *et al.*, Opt. Lett. **21**, 62 (1996).
[17] A. Brodeur *et al.*, Opt. Lett. **22**, 304 (1997).
[18] O. G. Kosareva *et al.*, Opt. Lett. **22**, 1332 (1997).
[19] L. Wöste *et al.*, Laser und Optoelektronik **29**, 51 (1997).
[20] B. La Fontaine *et al.*, Phys. Plasmas **6**, 1615 (1999).
[21] M. Mlejnek, E. M. Wright, and J.V. Moloney, Opt. Lett. **23**, 382 (1998).
[22] D. von der Linde and H. Schüler, J. Opt. Soc. Am. B **13**, 216 (1996).
[23] P. Audebert *et al.*, Phys. Rev. Lett. **73**, 1990 (1994).
[24] L.V. Keldysh, Sov. Phys. JETP **20**, 1307 (1965).
[25] M. Lenzner *et al.*, Phys. Rev. Lett. **80**, 4076 (1998).
[26] L. Sudrie, M. Franco, B. Prade, and A. Mysyrowicz, Opt. Commun. **191**, 333–339 (2001).
[27] E. Yablonovitch and N. Bloembergen, Phys. Rev. Lett. **29**, 907 (1972); N. Bloembergen, IEEE J. Quantum Electron. **QE-10**, 375 (1974).
[28] K. K. Thornber, J. Appl. Phys. **52**, 279 (1981).
[29] D. Du *et al.*, Appl. Phys. Lett. **64**, 3071 (1994).
[30] A.-C. Tien *et al.*, Phys. Rev. Lett., **82**, 3883 (1999).